Field-Calibrated Aerodynamic and Electromechanical Dynamic Simulation of a Bergey Excel 15 Wind Turbine for Distributed Generation

Jorge A. Leon Quiroga*, Luis E. Rodriguez-Rodriguez†, Rachid Darbali-Zamora*, Erick E. Aponte-Bezares†
*Sandia National Laboratories, Albuquerque, New Mexico, 87185, USA
†University of Puerto Rico-Mayagüez, Mayagüez, Puerto Rico 00680, USA

2025 Resilience Week (RWS) | 979-8-3315-5687-7/25/$31.00 ©2025 IEEE | DOI: 10.1109/RWS66711.2025.11304441

***Abstract*—This paper presents a modeling and control framework for the Bergey Excel 15, a 15-kW small-scale wind turbine designed for distributed energy applications. The system is modeled in MATLAB®/Simulink® and includes detailed representations of the aerodynamic subsystem, permanent magnet synchronous generator (PMSG), power electronics, and control algorithms. This work introduces a robust method to estimate the power coefficient curve $C_p(\lambda)$ from field data corrected for turbulence and sensor noise, yielding a physically consistent lookup table for aerodynamic torque calculation. The electrical subsystem consists of a back-to-back converter with dq-frame current control. The generator-side controller implements maximum power point tracking (MPPT) through speed regulation at the optimal tip-speed ratio. The grid-side controller maintains the DC-link voltage and regulates both active and reactive power exchange with the grid. The model enables real-time dynamic simulations and supports integration studies for microgrids and off-grid applications. Simulation results validate the effectiveness of the proposed approach and demonstrate its capability to capture the key dynamics of the Bergey Excel 15 DW turbine under variable wind conditions.**

***Index Terms*—Distributed Energy Resources (DERs), Permanent Magnet Synchronous Generator (PMSG), Maximum Power Point Tracking (MPPT), Grid Integration, Renewable Energy System**

I. Introduction

The increasing deployment of Distributed Energy Resources (DERs) has enabled localized power generation, enhanced resilience, and accelerated the transition to a more reliable energy infrastructure [1]. Distributed Wind (DW) turbines are small-scale wind energy systems designed to generate electricity for local consumption, ideal for residential homes, farms, and remote communities. These systems reduce transmission losses, support grid flexibility, and can provide backup power during outages or grid disturbances. Most DW turbines feature a mechanically robust design that enables reliable operation under diverse environmental conditions, making them suitable for integration into grid-connected [2], [3], hybrid microgrid [4], [5], and fully off-grid systems [6], [7].

The development of accurate simulation models for DW turbines is crucial for understanding their performance and optimizing their integration into the electric grid. Comprehensive models help evaluate system stability, grid support capabilities, and power quality under realistic operating conditions. Key components of these systems include an aerodynamic subsystem, a generator, an active rectifier, and a grid-tied inverter. The aerodynamic model captures rotor efficiency and dynamic torque response, while the generator model represents the electrical and electromechanical behavior of the system under varying loads. The active rectifier regulates power flow from the generator to the DC link, and the inverter ensures grid-compatible voltage [8], [9], and frequency regulation [10]. The model integrates control functionalities such as Maximum Power Point Tracking (MPPT) and reactive power regulation to evaluate system behavior under variable wind and grid conditions.

A critical factor in maximizing energy capture is the use of the power coefficient curve $C_p(\lambda)$, which defines aerodynamic efficiency as a function of the tip-speed ratio. Studies have demonstrated both analytical and real-time estimation techniques for $C_p(\lambda)$ to enhance MPPT performance [11]. Recent work has shown that coupling aerodynamic models with electromagnetic transient simulations and incorporating wind speed estimation via Kalman filtering can improve torque, speed, and power prediction accuracy [12]. These findings highlight the importance of validated, physics-based models and field-calibrated $C_p(\lambda, \beta)$ curves, which are directly relevant to the development of DW simulation frameworks. In addition, modeling approaches that integrate field-measured data can help account for turbulence, measurement uncertainty, and site-specific effects.

Although significant progress exists in the modeling of utility-scale wind energy conversion systems, detailed simulation modeling of distributed wind (DW) turbines remains limited. Most studies model large turbines under steady inflow, simplifying aerodynamic and electrical interactions. In contrast, DW turbines experience highly variable inflow turbulence, rapid wind speed transients, and strong nonlinear coupling between the rotor, generator, and power electronics stages. These conditions demand high-fidelity, field-calibrated models capable of representing dynamic interactions, control response, and power conversion efficiency across a wide range of operating points. Neglecting these characteristics can lead to inaccurate performance prediction, improper controller tuning, and incomplete system-level integration analyses for DW turbines.

Herein, this paper presents a validated, MATLAB®/Simulink®-based simulation model of a DW energy system. The model integrates aerodynamic,

Authorized licensed use limited to: Sandia National Laboratories. Downloaded on January 06,2026 at 07:14:31 UTC from IEEE Xplore. Restrictions apply.

electromechanical, and power electronic subsystems using parameters and performance data obtained from a commercially available DW turbine. The aerodynamic subsystem derives from experimental measurements of wind speed, rotor speed, and electrical power collected from an operating turbine. A robust, energy-based estimation approach derives a physically consistent $C_p(\lambda)$ curve corrected for turbulence and sensor noise, enabling accurate computation of aerodynamic torque across varying wind conditions. This calibration approach enhances physical fidelity compared to purely analytical or manufacturer-based performance curves and captures realistic variations in energy extraction efficiency. Similar hybrid approaches combining field data and aerodynamic modeling have demonstrated improved accuracy in predicting small wind turbine performance and control behavior.

The electrical subsystem consists of a Permanent Magnet Synchronous Generator (PMSG), an active bridge rectifier, a DC-link capacitor, and a grid-side inverter. The active rectifier regulates generator output current to control energy flow into the DC link, while the inverter converts DC power into AC for grid injection. The inverter control maintains DC-link voltage stability and includes functionality to manage reactive power exchange with the grid, enabling efficient power conversion.

Simulation results are validated using field data collected from a Bergey Excel 15, a commercially available DW turbine. The comparison includes time-domain and steady-state analysis of aerodynamic power, rotor speed, and electrical power. Results demonstrate a strong correlation between simulated and measured performance, confirming that the proposed models accurately capture the dynamic responses of the turbine and its control system.

II. System Configuration and Numerical Model

This work focuses on the modeling and simulation of the Bergey Excel 15, a small-scale horizontal-axis wind turbine designed for residential, agricultural, and remote power applications. The turbine is rated at 15 kW, operates at variable speed, and uses a fixed-pitch rotor with a three-phase PMSG. The grid-side converter is a single-phase inverter with an operating voltage of 120V. The system configuration is shown in Fig. 1.

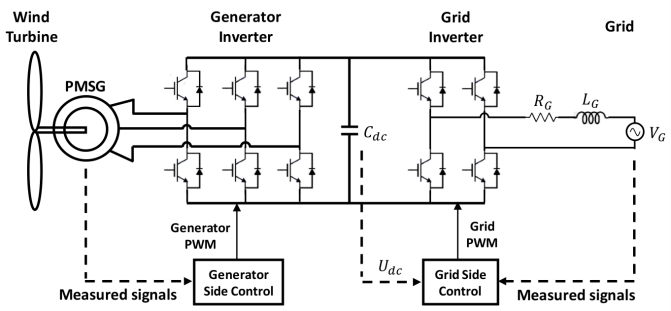

Fig. 1. Bergey Excel 15 DW system configuration.

A. Aerodynamic Model

The aerodynamic model of the turbine is developed based on the power coefficient curve $C_p(\lambda)$, which characterizes the efficiency of the rotor in extracting energy from the wind. The aerodynamic power extracted by the turbine is given by:

$$P_a = \frac{1}{2}\rho A C_p(\lambda) v^3 \tag{1}$$

where ρ is the air density, $A = \pi R^2$ is the swept area of the blades, and v is the wind speed. The tip-speed ratio λ is defined as:

$$\lambda = \frac{\omega R}{v} \tag{2}$$

where ω is the rotor angular velocity and R is the blade radius. The aerodynamic torque is then computed as:

$$T_a = \frac{P_a}{\omega} \tag{3}$$

The $C_p(\lambda)$ curve used in this model is derived from field-measured performance data and is implemented in Simulink via a lookup table, allowing for dynamic calculation of the aerodynamic torque under varying wind conditions.

To estimate the $C_p(\lambda)$ curve, field data were collected from an operating Bergey Excel 15 turbine, including time series measurements of wind speed, rotor shaft speed, and electrical and mechanical power output. Direct computation of C_p from instantaneous measurements is known to be highly sensitive to sensor noise, temporal misalignment, and turbulent fluctuations, often resulting in nonphysical values above the Betz Limit. To overcome these limitations, a robust estimation strategy based on energy integration and corrected wind speed was used.

First, the wind speed measurements were corrected to estimate the effective undisturbed wind speed at the rotor plane. The correction was derived from a momentum-based rearrangement of the wind power equation:

$$v_{\text{corr}} = \frac{P_{\text{gen}}}{2\rho A v_m^2} + v_m \tag{4}$$

where P_{gen} is the measured electrical power, V_m is the measured wind speed, and V_{corr} is the corrected wind speed. This correction accounts for the kinetic energy extracted by the rotor, improving the accuracy of the estimated inflow conditions. This approach was explained in detailed by J. Dai et al. [13].

To determine the power coefficient, the time series data were divided into intervals (e.g., 30 - 60 seconds), and an energy balance was applied to each interval to eliminate sensor noise, temporal misalignment, and turbulent fluctuations. The total aerodynamic energy extracted during an interval $[t_0, t_1]$ was calculated as follows:

$$E_{\text{aero}} = \int_{t_0}^{t_1} P_{\text{gen}}(t)\, dt + \frac{1}{2} J \left[\omega(t_1)^2 - \omega(t_0)^2\right] \tag{5}$$

Authorized licensed use limited to: Sandia National Laboratories. Downloaded on January 06,2026 at 07:14:31 UTC from IEEE Xplore. Restrictions apply.

where the first term accounts for the energy harvested by the turbine, J is the total moment of inertia of the turbine and generator, and the second term accounts for the change in rotational kinetic energy of the system.

The total wind energy available over the same interval was computed using the corrected wind speed:

$$E_{\text{wind}} = \int_{t_0}^{t_1} \frac{1}{2}\rho A v_{\text{corr}}(t)^3 \, dt \tag{6}$$

The average power coefficient for that interval was then obtained as:

$$\bar{C}_p = \frac{E_{\text{aero}}}{E_{\text{wind}}} \tag{7}$$

To associate each $\bar{C}_p$ with a representative tip-speed ratio, an energy-equivalent wind speed was calculated for each interval as:

$$V_{\text{eq}} = \left(\frac{\int_{t_0}^{t_1} \rho V_{\text{corr}}(t)^3 \, dt}{\int_{t_0}^{t_1} \rho \, dt} \right)^{1/3} \tag{8}$$

This formulation ensures that V_{eq} captures the dominant energetic contribution of fluctuating wind speed during the interval, rather than a simple arithmetic mean. The equivalent tip-speed ratio was then computed as:

$$\bar{\lambda} = \frac{\omega_{\text{eq}} R}{V_{\text{eq}}} \tag{9}$$

where ω_{eq} is taken as the average shaft speed over the interval, converted from RPM to rad/s, and R is the rotor radius. While an energy-based averaging was applied to the wind speed to compute V_{eq}, a simpler arithmetic mean was used for the rotor speed. This choice was justified by the observation that wind speed typically exhibits higher variability and stronger nonlinear influence on aerodynamic power than the relatively smoother rotor speed signal. This method ensures a physically consistent and energetically weighted estimate of the operating conditions for each $(\bar{\lambda}, \bar{C}_p)$ pair.

This procedure was repeated over multiple intervals across different wind conditions, resulting in a dataset of $(\bar{\lambda}, \bar{C}_p)$ pairs. These data points were then used to construct a smoothed $C_p(\lambda)$ curve, which was implemented in Simulink as a lookup table. This enables real-time computation of the aerodynamic torque under dynamic wind conditions while preserving physical consistency with measured turbine behavior. The C_p curve calculated from the experimental data is presented in Fig. 2.

B. Power Electronics Model

The electrical subsystem of the Bergey Excel 15 wind turbine is represented by a full-conversion topology consisting of a three-phase Permanent Magnet Synchronous Generator (PMSG), a generator-side inverter, a DC-link capacitor, and a grid-side inverter interfaced with the grid, as shown in Fig. 1. Following the approach adopted in prior works on average-value modeling of renewable energy conversion systems [14],

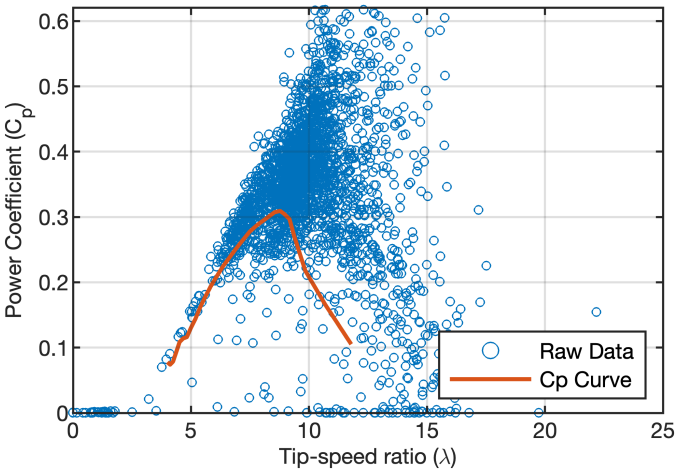

Fig. 2. Cp Curve calculated from field data for a Bergey turbine.

[15], this study neglects high-frequency switching harmonics while preserving the fundamental power conversion dynamics. Such averaged representations significantly reduce computational complexity, making the model suitable for system-level control design and validation.

The PMSG is modeled in the dq synchronous reference frame aligned with the rotor flux, which simplifies the representation of the machine dynamics. The stator current dynamics are expressed as:

$$\frac{di_d}{dt} = \frac{1}{L_d}\left(V_d + \omega_e L_q i_q - R_s i_d\right) \tag{10}$$

$$\frac{di_q}{dt} = \frac{1}{L_q}\left(V_q - \omega_e L_d i_d - R_s i_q - \omega_e \lambda_m\right) \tag{11}$$

where i_d and i_q are the stator currents in the $d-$ and $q-$axes, V_d and V_q are the corresponding terminal voltages, R_s is the stator resistance, L_d and L_q are the stator inductances, ω_e is the rotor angular speed, and λ_m is the flux linkage produced by the permanent magnets.

The electromagnetic torque is obtained from the standard expression in the dq- frame:

$$T_e = \frac{3}{2} P \left(\lambda_m i_q + (L_d - L_q) i_d i_q\right) \tag{12}$$

where P is the number of pole pairs. These equations establish the dynamic model of the PMSG in the dq-frame, serving as the electrical input to the converter subsystem.

The generator-side inverter converts the three-phase AC output of the PMSG into DC and is represented as a controllable voltage source that imposes the reference voltages V_d and V_q generated by the control system. The DC-link couples the generator-side and grid-side inverters, and is modeled as an ideal capacitor:

$$C_{dc} \frac{dU_{dc}}{dt} = i_{gen} - i_{grid} \tag{13}$$

Authorized licensed use limited to: Sandia National Laboratories. Downloaded on January 06,2026 at 07:14:31 UTC from IEEE Xplore. Restrictions apply.

where U_{dc} is the DC-link voltage, i_{gen} is the current injected by the generator-side inverter, i_{grid} is the current drawn by the grid-side inverter, and C_{dc} is the DC-link capacitance.

The grid-side inverter converts the DC power back into AC for injection into the utility grid. The grid connection is modeled with a series filter composed of an inductance L_G and resistance R_G. The dynamic equation at the point of common coupling (PCC) is:

$$L_G \frac{di_g}{dt} + R_G i_g = V_{inv}(t) - V_g(t) \tag{14}$$

where i_g is the current injected into the grid, $V_{inv}(t)$ is the inverter output voltage, and $V_g(t)$ is the instantaneous grid voltage. These averaged equations described the interaction between the converter stages and provide the electrical interface for the contol system design discussed in the next section.

C. Control Algorithm

The control strategy implemented for this work is based on the vector control architecture described in [16], and it is illustrated in Fig. 1. The system employs a decoupled, back-to-back control structure that independently regulates the generator-side and grid-side converters using synchronous reference frame control.

1) Generator-Side Control: The generator-side converter applies Field-Oriented Control (FOC) to regulate the PMSG torque and extract maximum power from the wind. The stator currents are expressed in the dq synchronous frame aligned with the rotor, allowing independent control of flux and torque. For efficient operation, the d-axis current reference is set to zero, which aligns the stator flux with the permanent magnet flux and ensures operation at unity power factor.

The torque-producing q-axis current reference, i_{sq}^*, is determined from the turbine's speed characteristic. Rather than directly tracking electrical power output, the control strategy regulates the rotor speed at its optimal value, which corresponds to the maximum power coefficient C_p. In theory, this optimal operating point is defined by maintaining the tip-speed ratio λ_{opt}, leading to the speed reference:

$$\omega_{\text{ref}} = \frac{\lambda_{\text{opt}} \cdot v_{\text{wind}}}{R} \tag{15}$$

where v_{wind} is the wind speed and R is the turbine blade radius. In practice, this relationship is implemented in the model through a lookup table constructed from turbine performance data, which maps the aerodynamic power to the corresponding optimal rotor speed.

The resulting speed reference ω_{ref} is then used as the input to a PI controller that regulates the torque-producing q-axis stator current reference i_{sq}^*, ensuring that the generator torque drives the rotor toward the optimal aerodynamic operating point. The reference $q-$axis current in the frequency domain is expressed as:

$$i_{sq}^* = (K_{p,gen} + K_{i,gen}\frac{1}{s})(\omega_{ref} - \omega) \tag{16}$$

where $K_{p,gen}$ and $K_{i,gen}$ are the proportional and integral gains of the speed controller. The inner current control loops for both $d-$ and $q-$axes are implemented using PI regulators which compares the measured stator currents with their reference ($i_d^* = 0$, i_q^*) and generate the voltage commands v_{sd}^* and v_{sq}^*. These voltage references are then transformed back to the abc frame and directly applied to the converter in average mode.

2) Grid-Side Control: The grid-side converter is regulated in the synchronous dq reference frame control aligned with the grid voltage vector, as determined by a PLL. The control objectives are twofold: (i) to regulate the DC-link voltage through the active power channel, and (ii) to manage reactive power exchange with the grid.

The outer voltage controller compares the measured DC-link voltage U_{dc} with its reference U_{dc}^*, and generates the $d-$axis current reference:

$$i_d^* = (K_{p,dc} + K_{i,dc}\frac{1}{s})(U_{dc}^* - U_{dc}) \tag{17}$$

where $K_{p,DC}$ and $K_{i,DC}$ are the proportional and integral gains of the DC voltage controller. Similarly, the $q-$axis current reference is generated to regulate the desired reactive power exchange with the grid:

The d-axis current i_d controls the active power, while the q-axis current i_q regulates reactive power. The current references i_d^* and i_q^* are generated from outer PI controllers as:

$$i_q^* = (K_{p,Q} + K_{i,Q}\frac{1}{s})(Q_{ref} - Q) \tag{18}$$

where Q_{ref} is the reactive power reference and Q is the measured reactive power.

The inner current control loops are implemented as PI controllers that track the i_d^* and i_q^* references, producing the voltage commands V_d^* and V_q^*. These are then transformed back to the abc frame and directly applied to the averaged inverter model, which represents the grid-side converter in the simulation.

These control strategies enable maximum power extraction, DC-link voltage regulation and reactive power support. Their performance is evaluated in the simulation results that follow.

III. Simulation Results and Validation

To validate the proposed dynamic model and control strategy for the Bergey Excel 15 wind turbine, simulation results are compared against field measurements from an operational turbine. The validation focuses on both time-domain responses-rotor speed, aerodynamic Power, and inverter output-and steady-state characteristics, namely the Power vs. Wind and Shaft Speed vs. Power relationships. This combined analysis demonstrates the model's ability to reproduce the turbine's dynamic behavior and long-term operating trends.

Authorized licensed use limited to: Sandia National Laboratories. Downloaded on January 06,2026 at 07:14:31 UTC from IEEE Xplore. Restrictions apply.

A. *Time-Domain Performance*

Time-domain simulation results are obtained from the simulation model and compared with field data for the mechanical power, shaft speed and electrical power.

Fig. 3 shows the time series of mechanical (aerodynamic) power obtained from both the field data and the simulation model. The simulated response replicates the overall trend of the field measurements, capturing long-term wind resource variations as well as short-term fluctuations. Peak values are slightly underestimated, mainly due to the simplified wind input and the absence of a detailed turbulence model. Nevertheless, the agreement in mean levels and temporal dynamics demonstrates that the aerodynamic subsystem and the applied control strategy realistically represent turbine power capture.

Fig. 4 presents the shaft speed time series acquired from field measurements and the simulation model. The simulated response closely follows the measured shaft speed throughout the entire time window, indicating that the control strategy effectively regulates rotor dynamics under varying wind conditions. Minor discrepancies appear, primarily due to short-term fluctuations and measurement noise in the field data, which are not explicitly modeled. Overall, the agreement confirms that the proposed control scheme maintains the rotor near its optimal operating point.

Fig. 5 provides the inverter electrical power time series, comparing the simulated output of the averaged converter model with field measurements from the operational turbine. The simulated response matches the measured inverter power well, reproducing both the overall trend and the variability induced by wind fluctuations. Peak power events are slightly underestimated, in line with the aerodynamic power results, mainly due to the simplified wind input and the averaged

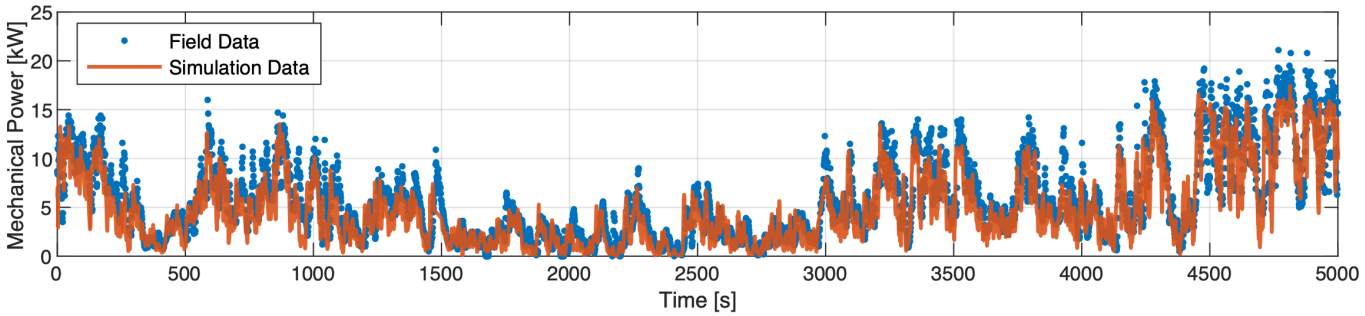

Fig. 3. Mechanical power time series: field and simulation data.

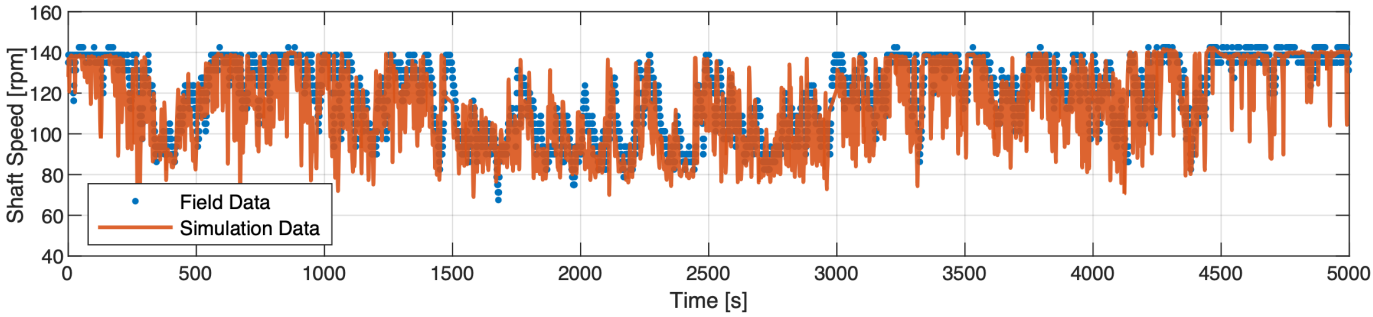

Fig. 4. Shaft speed time series: field and simulation data.

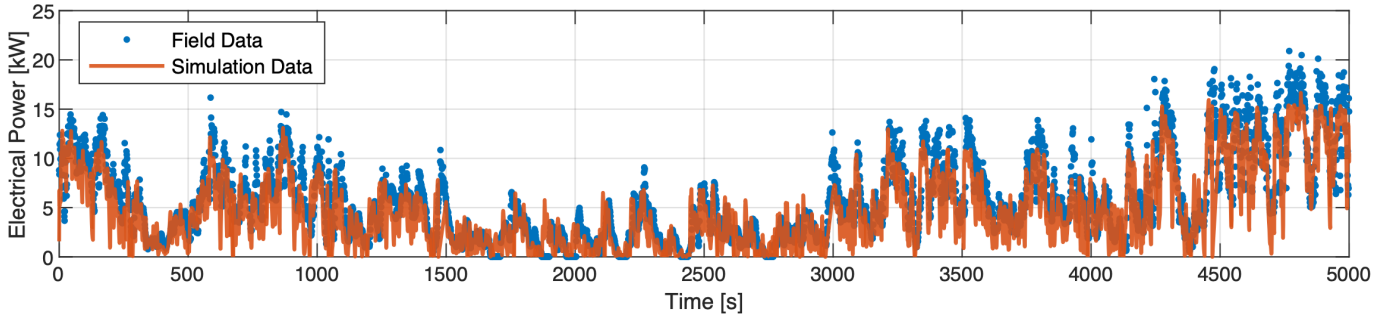

Fig. 5. Inverter electrical power time series: field and simulation data.

Authorized licensed use limited to: Sandia National Laboratories. Downloaded on January 06,2026 at 07:14:31 UTC from IEEE Xplore. Restrictions apply.

converter representation. Overall, this comparison confirms that the proposed model captures the electrical conversion process and reliably represents the power delivered to the grid.

After validating the time-domain responses, the analysis turns to steady-state characteristics, focusing on the Power vs Shaft Speed and Power vs. Wind Speed relationships.

B. Shaft Speed vs. Mechanical Power

Fig. 6 compares shaft speed against mechanical Power using three datasets: field measurements, simulation results, and fitted power curves. The field data (blue) exhibit significant dispersion, reflecting turbulence and transient effects. The simulation results (orange) form a tighter distribution, clustering around the expected steady-state trajectory. The fitted field curve (green) and the corresponding simulation curve (purple) both capture the nonlinear relationship between shaft speed and Power, with good agreement across most of the operating range. Minor deviations at higher speeds are attributed to the limited availability of field measurements beyond 140 rpm. Overall, this comparison confirms that the aerodynamic model and the control strategy consistently drives the rotor along the optimal power-speed characteristic.

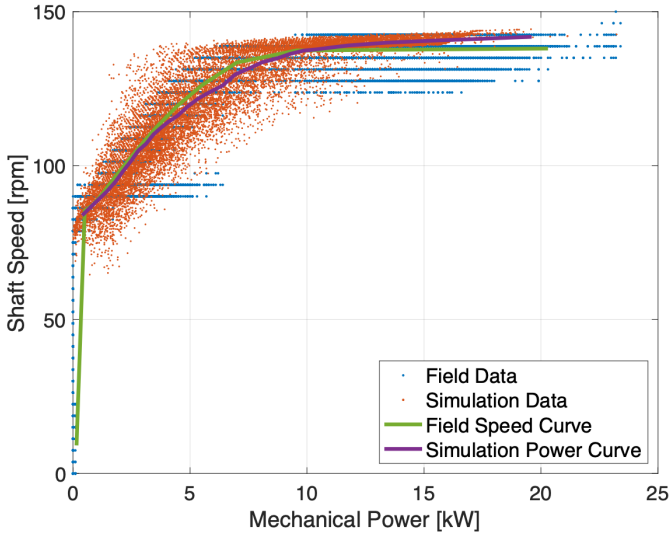

Fig. 6. Shaft speed vs. mechanical power: field, simulation, and fitted curves.

C. Power Vs. Wind Speed

Fig. 7 shows the relationship between wind speed and mechanical Power for field data, simulation results, and the corresponding fitted curves. The field data (blue) display a wide dispersion caused by turbulence and measurement variability, while the simulation results (orange) form a narrower band that aligns with the central tendency of the field distribution. The fitted curves derived from the field measurements (green) and from the simulation (purple) show strong agreement across the central operating region. At higher wind speeds, deviations become more evident, which is attributed to the aerodynamic models being calibrated in the mid-range of operation rather than extremes. Overall, the comparison demonstrates that the model captures the average power-wind relationship with good fidelity.

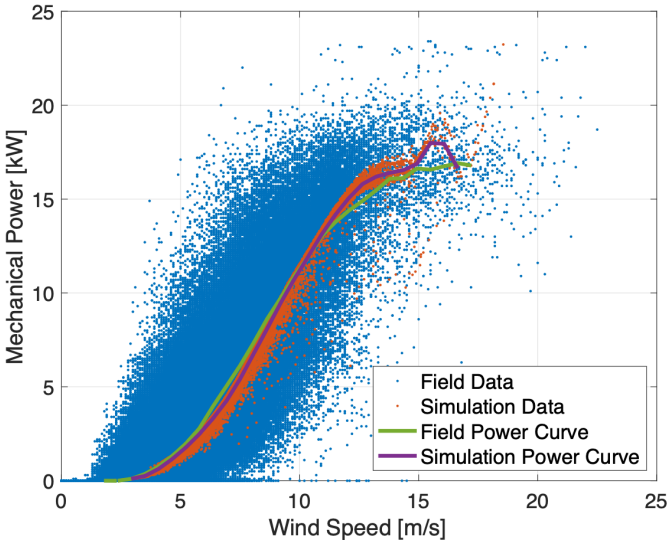

Fig. 7. Mechanical power vs. wind speed: field, simulation, and fitted curves.

These results demonstrate that the proposed modeling framework and control strategy provide a realistic and physically consistent representation of the Bergey Excel 15 turbine dynamics. The validated model supports future applications in grid integration studies, system optimization, and controller prototyping for small-scale wind energy systems.

IV. Conclusions

This paper presents a validated modeling and control framework for the Bergey Excel 15 wind turbine, designed for system integration applications. The model combines aerodynamic, electrical, and control subsystems into a single system, enabling realistic simulation of the wind turbine's dynamic response under variable wind conditions. A key contribution of this work is the development of a calibrated $C_p(\lambda)$ curve using field data. This approach corrects wind speed to the rotor plane and incorporating variations in rotor kinetic energy, this approach provides a more accurate aerodynamic performance model. This approach allows simulation testing of different control models.

The simulations results replicate dynamic behavior of the wind turbine and show similar responses to the field data measurements in both dynamic responses and steady-state characteristics. This indicates that the aerodynamic, electrical, and control subsystems interact consistently. Additionally, the dynamics in the active rectifier and the inverter are able to control stable DC-link regulation and electrical power delivery, respectively.

This modeling approach provides a platform for control design, performance evaluation, and integration studies of small wind turbines.

Authorized licensed use limited to: Sandia National Laboratories. Downloaded on January 06,2026 at 07:14:31 UTC from IEEE Xplore. Restrictions apply.

Acknowledgement

This article has been authored by an employee of National Technology & Engineering Solutions of Sandia, LLC under Contract No. DE-NA0003525 with the U.S. Department of Energy (DOE). The employee owns all right, title and interest in and to the article and is solely responsible for its contents. The U.S. Government retains and the publisher, by accepting the article for publication, acknowledges that the U.S. Government retains a non-exclusive, paid up, irrevocable, worldwide license to publish or reproduce the published form of this article or allow others to do so, for U.S. Government purposes. The DOE will provide public access to these results of federally sponsored research in accordance with the DOE Public Access Plan.

The authors would like to acknowledge the financial support provided by the U.S. DOE, Office of Energy Efficiency (EERE), Wind Energy Technology Office (WETO) for the Wind Hybrid Integration Platform (WHIP) project under Work Breakdown Structure No. 1.2.6.701 as well as the contributions from Bret Barker and Patrick Gilman.

References

[1] M. Kanabar and C. Cosoreanu, "Building the grid of the future to accelerate energy transition: Innovations and digital transformation for global utilities," *IEEE Power and Energy Magazine*, vol. 22, no. 2, pp. 90–99, 2024.

[2] M. Jimenez-Aparicio and R. Darbali-Zamora, "Reactive power control for fast-acting voltage regulation of distributed wind turbines using reinforcement learning," in *2023 IEEE Kansas Power and Energy Conference (KPEC)*, 2023, pp. 1–6.

[3] M. Jimenez-Aparicio, R. Darbali-Zamora, "Cooperative multi-agent reinforcement learning method for fast voltage regulation using distributed wind turbine generators," in *2023 IEEE PES Innovative Smart Grid Technologies Latin America (ISGT-LA)*, 2023, pp. 1–5.

[4] J. Choi, J. E. Quiroz, R. T. Brito, R. Darbali-Zamora, E. E. Aponte-Bezares, and M. S. Lave, "An assessment of wind-hybrid microgrids in puerto rico using microgrid design toolkit," in *2024 56th North American Power Symposium (NAPS)*, 2024, pp. 1–6.

[5] R. J. Tremont-Brito, J. Choi, J. E. Quiroz, R. Darbali-Zamora, E. E. Aponte-Bezares, and M. S. Lave, "Microgrid design toolkit optimization of wind-pv hybrid microgrids for energy resilience in puerto rico," in *2025 IEEE 53rd Photovoltaic Specialists Conference (PVSC)*, 2025, pp. 1597–1604.

[6] M. Jimenez-Aparicio and R. Darbali-Zamora, "Increasing the penetration of distributed wind in an isolated microgrid through data-driven frequency regulation using reinforcement learning," in *2024 IEEE Kansas Power and Energy Conference (KPEC)*, 2024, pp. 1–6.

[7] J. B. VanderMeer, N. Green, R. Darbali-Zamora, and W. Thompson, "Microgrid renewable integration dispatch and sizing (migrids) analysis of spinning and regulating reserve options for wind in an alaskan diesel microgrid," *IEEE Access*, vol. 11, pp. 121 637–121 645, 2023.

[8] R. Darbali-Zamora, S. T. Ojetola, F. Wilches-Bernal, and J. C. Berg, "Development of a wind turbine generator volt-var curve control for voltage regulation in grid connected systems," in *2022 North American Power Symposium (NAPS)*, 2022, pp. 1–6.

[9] R. Darbali-Zamora and J. C. Berg, "Development of a wind turbine generator volt-var curve control for voltage regulation using power hardware-in-the-loop," in *2023 IEEE PES Innovative Smart Grid Technologies Latin America (ISGT-LA)*, 2023, pp. 280–284.

[10] F. Wilches-Bemal, R. Darbali-Zamora, B. T. Naughton, and J. D. Flicker, "Model characterization and frequency regulation in wind-diesel hybrid microgrids," in *2022 North American Power Symposium (NAPS)*, 2022, pp. 1–5.

[11] C. Lumbreras, J. M. Guerrero, P. García, F. Briz, and D. D. Reigosa, "Control of a small wind turbine in the high wind speed region," *IEEE Transactions on Power Electronics*, vol. 31, no. 10, pp. 6980–6991, 2016.

[12] G. E. North Piegan, R. Darbali-Zamora, and J. C. Berg, "Development and validation of a wind turbine generator simulation model," in *2022 North American Power Symposium (NAPS)*, 2022, pp. 1–6.

[13] J. Dai, D. Liu, L. Wen, and X. Long, "Research on power coefficient of wind turbines based on scada data," *Renewable Energy*, vol. 86, pp. 206–215, 2016.

[14] Q. Zhang, J. He, Y. Xu, Z. Hong, Y. Chen, and K. Strunz, "Average-value modeling of direct-driven pmsg-based wind energy conversion systems," *IEEE Transactions on Energy Conversion*, vol. 37, no. 1, pp. 264–273, 2022.

[15] G. Rajeshree, B. Nived, G. Revati, and R. Meshram, "Model reference adaptive control-based modelling of rectifier and inverter," in *2023 European Control Conference (ECC)*, 2023, pp. 1–6.

[16] M. N. Eskander and A. M. Massoud, "Vector control strategy for small-scale grid-connected pmsg wind turbine converter," *Alexandria Engineering Journal*, vol. 51, no. 2, pp. 123–132, 2012.

Authorized licensed use limited to: Sandia National Laboratories. Downloaded on January 06,2026 at 07:14:31 UTC from IEEE Xplore. Restrictions apply.